http://dx.doi.org/10.5012/bkcs.2013.34.3.957

Photodissociation Dynamics of C_6F_5Br at 234 nm: Fluorination Effects on Br/Br* Formation Pathways

Dababrata Paul, Hyun Kook Kim, and Tae Kyu Kim*

Department of Chemistry and Chemical Institute for Functional Materials, Pusan National University, Busan 609-735, Korea
**E-mail: tkkim@pusan.ac.kr*
Received November 21, 2012, Accepted December 9, 2012

Key Words : Aryl halide, Photodissociation, Ion-imaging, Potential energy surface

Photodissociation dynamics of organic halides has been extensively investigated due to its potential to the stratosphere ozone depletion and relevant environmental problems. For example, alkyl bromide as the simplest organic halides has been used for model of photodissociation dynamics. The A-band of alkyl bromide arises from the C–Br bond localized $\sigma^* \leftarrow n$ transition and consists of three overlapping transitions to repulsive states ($^3Q_1$, $^3Q_0$, and $^1Q_1$: on ascending order of excitation energy). The dominant transition in the A-band is to the $^3Q_{0+}$ state which correlates to the $Br^*(^2P_{1/2})$ products, suggesting the spin-orbit ground $Br(^2P_{3/2})$ atom formation arises as a results of nonadiabatic coupling between the $^3Q_{0+}$ and $^2Q_1$ PESs *via* a conical intersection along the C–Br bond coordinate.[4-6]

Compared to the photodissociation of alkyl bromide, the photodissociation dynamics of aryl halides[7-16] show more complicated because more electronic states are involved and thus making multiple dissociation pathways probable. Multiple dissociation pathways include the predissociation between excited electronic states, internal conversion processes from vibrational excited states, and dissociation processes from repulsive states. It has been unraveled by numerous studies that dissociation pathways are substantially dependent on the type of halogen,[9-11] atomic substituents,[12] and excitation wavelengths.[13] In the early work on the bromobenzene (C_6H_5Br) photodissociation near 266 nm,[7-12,14] the main dissociation channel is an indirect dissociation involving the bound (π, π^*) and repulsive (π, σ^*) states. In the short wavelength, significant UV absorption of bromobenzene is caused by $\sigma^* \leftarrow n$ and $\pi^* \leftarrow \pi$ transition; the mixing between these states becomes more probable and additional routes can be observed as in the case of photodissociation of iodobezene.[8,14] With the purpose of elucidation of dissociation dynamics of bromobenzene at short-wavelengths, we have previously investigated 234 nm dissociation dynamics of bromobenzene using velocity ion map imaging.[14] Observed trimodal translational distributions for Br/Br* formation channels have been attributed to the direct and indirect dissociation mechanisms originating from the initially excited (π, π^*) state. This is indicative that dissociation mechanisms of bromobenzene at 234 nm are more complicated than those near 270 nm.[14] In this regards, more systematic studies focused on effects of atomic substituents such as fluorine, bromine and chlorine on phenyl group are required to have a comprehensive understanding of the photodissociation dynamics of bromobenzene near 234 nm. The objective of the present work is to investigate the fluorine substitution effects in bromobenzene near 234 nm further. In this note, as continuing efforts for this purpose, we present ion-imaging study for photodissociation dynamics of pentafluorobromobenzen (C_6F_5Br) at 234 nm using velocity map imaging coupled with [2+1] resonance enhanced multiphoton ionization (REMPI) scheme. With aid of *ab initio* calculations,[9,12] detailed photodissocation pathways are discussed.

The velocity map imaging apparatus, similar to that used previously,[2,14] consists of molecular beam chamber and main interaction chamber with TOF spectrometer. Liquid samples of C_6F_5Br were used without further purification. Vapors of liquid C_6F_5Br (10-20 torr, 98.5%) were carried by helium gas at 1.5 atm through the pulsed value operating synchronously with the pulse laser at 10 Hz. Output laser pulses from the Nd:YAG pumped dye laser (HD500, Lumonics) were frequency-doubled to emit at 234 nm with an energy range of 50-150 μJ and subsequently focused onto the skimmed molecular beam with a 150 mm focal lens. C_6F_5Br molecules were dissociated and Br fragments were simultaneously ionized using [2+1] REMPI schemes.[17] With a set of ion-optics for the velocity map ion-imaging,[18] the Br^+ were expanded, accelerated by nonhomogeneous electric field and projected onto a 40 mm Chevron-type dual MCP coupled to phosphor screen. The transient image from the phosphor screen were taken by a charge-coupled device (CCD) camera. All timings of the pulsed value, Nd:YAG laser, and the gating pulse for MCP were manipulated by a multichannel delay generator. (SRS, DG535).

Upon irradiation at 234 nm, C_6F_5Br dissociates to release the Br/Br* photofragments. The resultant Br and Br* images resulting from 234 nm photolysis of C_6F_5Br are presented in Figures 1(a) and 1(b), respectively. Because each image is a 2D projection of 3D distribution of photofragments with cylindrical symmetry around laser polarization axis, the shape of an image is dependent on the speed (energy) and angular distributions of fragments.[18] From the measured images for Br and Br* channels, the speed distributions ($P(v)$) were extracted by integrating the 3D speed distribution over all angles at each speed, and subsequently the total translation

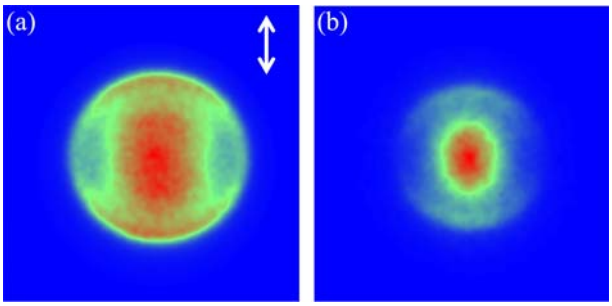

Figure 1. Raw ion images of Br and Br* from the photolysis of C_6F_5Br [(a), (b)]. In all images, the polarization of photolysis laser is vertically aligned.

energy distributions based on a center-of-mass coordinate, $P(E_T)$, were obtained by converting the speed distribution using equations: $P(E_T)dE = P(v)dv$ and $E_T = 1/2(m_{Br} + m_{C_6F_5})(m_{Br}/m_{C_6F_5})v_{Br}^2$. The total translational energy distributions for Br and Br* from C_6F_5Br are plotted in Figure 2. As we mentioned, from the photodissociation of C_6H_5Br at 234 nm, energy distributions of Br/Br* can be modeled by trimodal distributions. In contrast, in case of C_6F_5Br, total energy distributions of Br/Br* are well described by only two functions: one Boltzmann and single Gaussian distributions.

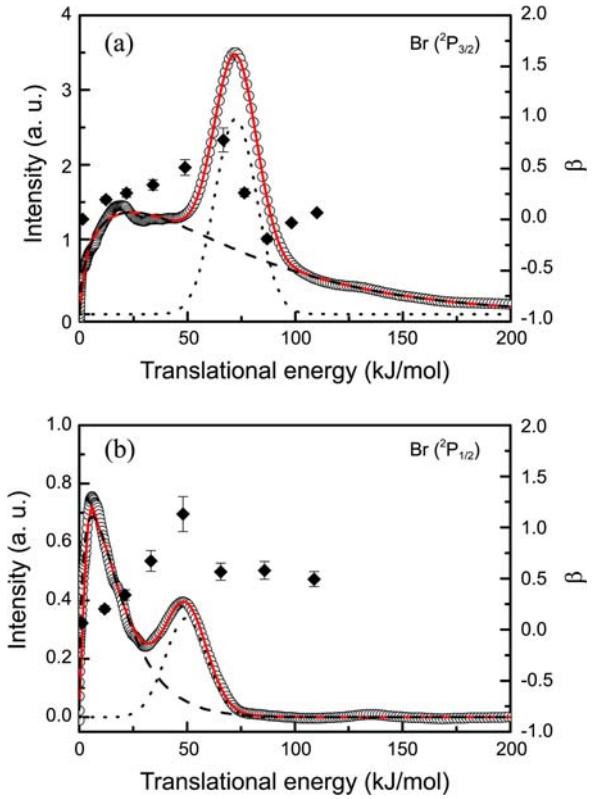

Figure 2. Total translational energy distributions of Br (a) and Br* (b) from photodissociation of C_6F_5Br near 234 nm. β values with error-bars corresponding to individual translational energy values are also displayed. Each data point (shown as open circle) corresponds to the relative signal intensity obtained by integrating values for all angular components at a specific translational energy. The anisotropy parameters (shown as filled diamonds in the axes on the right) are also displayed as a function of the translational energy.

Table 1. The branching ratios and relative quantum yields for the each translational energy components of C_6F_5 + Br(Br*) channels at 234 nm

Channel	Φ_{low}^{BZ}	Φ_{high}^{GA}	Φ_{TOTAL}
C_6F_5+Br	0.61	0.28	0.89
C_6F_5+Br*	0.07	0.04	0.11
Br*/Br	0.11	0.14	-

To assign each distribution, the recoil anisotropy parameter, β should be obtained by fitting angular distribution ($P(\theta)$) at certain energy range with the following formula: $P(\theta) = N(1 + \beta P_2(\cos\theta))$, where θ is the angle between the recoil velocity vector of the photofragments and the polarization axis of the laser, N is the proportional constant, and $P_2(\cos\theta)$ is the second-order Legendre polynomial.[19] The recoil anisotropy value corresponding to individual translational energy distribution was extracted and displayed in Figure 2. β values were found to vary from -0.24 to 0.76 in the case of Br and from 0.15 to 1.21 in the case of Br*, respectively. The relative quantum yields for Br and Br* were determined from the relative peak intensity of the TOF spectra. The resultant quantum yield were $\Phi(Br^*) = 0.11 \pm 0.01$ and $\Phi(Br) = 0.89 \pm 0.02$. Following these values, the relative quantum yields for each energy component in Figure 2 were extracted and are listed in Table 1.

On the earlier study of bromobenzene at 234 nm,[14] three possible dissociation mechanisms have been proposed: one is *via* direct dissociation along a repulsive $^{1,3}(\pi, \sigma^*)$ states as in cases of alkyl bromide dissociation through $^3Q_{0+}$ state, second is *via* fast predissociation occurs if the parent molecules are excited to bound $^1(\pi, \pi^*)$ state, crossing through a point that lies below the excitation energy to a repulsive $^{1,3}(\pi, \sigma^*)$ states, and the other is hot molecule dissociation *via* internal conversion from $^1(\pi, \pi^*)$ state. On contrary, the translational energy distributions of Br/Br* fragments from C_6F_5Br at the same wavelength, one Boltzmann distribution and single Gaussian function were required to best-fit distributions of Br and Br*. This suggests fluorine substitutions would influence the dissociation pathways of C_6H_5Br at 234 nm.[9,10,12] This might be attributed that the fluorination affects an energy ordering of low-lying electronic states. The translational energy distribution of Br (Br*) is well described by a Boltzmann shaped function peaked 20.2 (7.2) kJ/mol. In addition, isotropic angular distributions (in ideal case: β = 0.0) of fragments have been observed for both Br and Br*. The Boltzmann distributions as well as the isotropic angular distributions indicate that indirect dissociation through an electronic relaxation process followed by an internal conversion produces the Br and Br* for this velocity component.[16,20] In C_6H_5Br photodissociation study,[14] primary atomic bromine elimination following fast internal conversion from the excited electronic state to the ground state has been suggested for the origin for this velocity component. By analogy with the C_6H_5Br system, it is suggested that the low-velocity (Boltzmann) components observed in C_6F_5Br photodissociation originated from internal conversion from the

$^1(\pi, \pi^*)$ state to the vibrational excited ground state. Similar assignments have been suggested to the Boltzmann shape of the translation energy distributions of I/I^* from C_6H_5I and C_6F_5I at 304 nm.[21] It should be mentioned that the quantum yield for this process was calculated to be 0.68 (Table 1), indicating that this internal conversion process is much preferred. In C_6H_5Br photodissociation, ratio of 0.10 has been measured.[14]

A Gaussian shaped translational energy distribution has been observed. The relatively narrow distribution with low anisotropic angular distribution indicates fragments from this channel are originated from fast predissociation process. The average translational of Br and Br^* were found to be 75.2 and 51.1 kJ/mol, respectively. The relative fraction for this component of Br and Br^* was found to be 0.28 and 0.04, respectively. In C_6H_5Br photodissociation study at 234 nm, two probable channels for Gaussian distributions have been suggested: (1) direct bromine dissociation from repulsive $^3(\pi, \sigma^*)$ state and (2) bromine elimination from the curve-crossing from the initially excited $^1(\pi, \pi^*)$ state to the dissociative $^{1,3}(\pi, \sigma^*)$ states. To clarify the reaction pathway responsible for this velocity component, we infer *ab initio* CASSCF/CASPT2 quantum chemical calculations of fluorinated bromobenzenes.[9,10,12] Changes of energy ordering of low-lying electronic states have been confirmed: excitation energies of the lowest $\sigma^* \leftarrow \pi$ transition and triplet $\sigma^* \leftarrow n$ transition have been lowered and on the contrary, the $\pi^* \leftarrow \pi$ transition increases.[12] As a consequence, mixing of $^1(\pi, \pi^*)$ and $^3(n, \sigma^*)$ states becomes more probable and $^{1,3}(\pi, \sigma^*)$ states lie below the excitation energy (234 nm) at this study. This is indicative of an increased mixing of $^3(n, \sigma^*)$ character into the predominant $^1(\pi, \pi^*)$ transition in the Frank-Condon region at 234 nm. Based on previous calculations, it is suggested that high-velocity components with Gaussian shape observed in C_6F_5Br photodissociation originated from curve-crossing between $^1(\pi, \pi^*)$ and $^3(n, \sigma^*)$ states. On contrary to C_6H_5Br 234 nm case, the contribution of fast predissociation between $^1(\pi, \pi^*)$ and $^{1,3}(\pi, \sigma^*)$ states is negligible on fluorination. In addition, the fine-structure branching ratio, Br^*/Br, for this Gaussian component from C_6F_5Br (0.14) case is higher than in C_6H_5Br (0.08), indicating that the excited state Br^* is preferred. In the photodissociation of CH_3Br, fluorination reduces the curve-crossing probability between $^3Q_{0+}$ and $^1Q_1$ PESs.[2,22] The same analogy may be applied to Gaussian component from C_6F_5Br in the exit channels. If dissociation process occurs *via* $^3(n, \sigma^*)$ state, fluorination induces PESs diabatically to the excited state of Br.

Besides fluorination effects mentioned above, fluorinations on aryl group significantly increase quantum yield (0.68) for Boltzmann component than that (0.10) for C_6H_5Br dissociation. The curve-crossing between $^1(\pi, \pi^*)$ and $^3(n, \sigma^*)$ states is insufficient when electron density of π^* orbital localized on the conjugated C=C bonds is reduced. Thus, an observed quantum yield for Gaussian component from C_6F_5Br can be explained by reduced electron density in the π^* orbital by fluorine substituents. Similar phenomena have been found in the case of C_6H_5Cl and C_6F_5Cl at 193 nm.[15,20]

In summary, detailed dissociation mechanisms of 234 nm photodissociation of C_6F_5Br have been elucidated by using ion-imaging experimental results and *ab initio* calculations. The obtained translational energy distributions for both channels were well fitted by a single Boltzmann and one Gaussian functions The Gaussian component has been assigned to the predissociation between bound $^1(\pi, \pi^*)$ and repulsive $^3(n, \sigma^*)$ state. A slow internal conversion process followed by $^1(\pi, \pi^*)$ state excitation to the electronic ground state has been attributed to the origin of the Boltzmann component. Based on comparisons with C_6H_5Br dissociation mechanisms, several fluorination effects such as re-ordering of low-lying electronic states and reduced quantum yields have been discussed. Our group is planning to perform more systematic studies of photodissociation of bromobenzene at short wavelength.

Acknowledgments. This work was financially supported by the Research Fund Program of Research Institute for Basic Science, Pusan National University, Korea, 2010, Project No. RIBS-PNU-2010-106.

References

1. Sparks, R. K.; Shobadake, K.; Carlson, L. R.; Lee, Y. T. *J. Chem. Phys.* **1981**, *75*, 3838.
2. Kim, T. K.; Lee, K. W.; Lee, K. S.; Lee, E. K.; Jung, K. H. *Chem. Phys. Lett.* **2007**, *446*, 31.
3. Lee, K. S.; Lee, K. W.; Lee, S. K.; Jung, K. H.; Kim, T. K. *J. Mol. Spectra.* **2008**, *249*, 43.
4. Eppink, A. T. J. B.; Parker, D. H. *J. Chem. Phys.* **1999**, *110*, 832.
5. Zou, P.; McGiven, W. S.; North, S. W. *Phys. Chem. Chem. Phys.* **2000**, *2*, 3785.
6. Amatatsu, Y.; Yabushita, S.; Morokuma, K. *J. Chem. Phys.* **1996**, *104*, 9783.
7. Zhang, H.; Zhu, R. S.; Wang, G. J.; Han, K. L.; He, G. Z.; Lou, N. Q. *J. Chem. Phys.* **1999**, *110*, 2922.
8. Tang, B.; Zhu, R.; Tang, Y.; Ji, L.; Zhang, B. *Chem. Phys. Lett.* **2003**, *381*, 617.
9. Liu, Y. J.; Persson, P.; Karlsson, H. O.; Lunell, S.; Kadi, M.; Karlsson, D.; Davidsson, J. *J. Chem. Phys.* **2004**, *120*, 6502.
10. Chen, S. F.; Liu, F. Y.; Liu, Y. J. *J. Chem. Phys.* **2009**, *131*, 124304.
11. Zhang, X. P.; Wei, Z. R.; Tang, Y.; Chao, T. J.; Zhang, B.; Lin, K. C. *Chem. Phys. Chem.* **2009**, *9*, 1130.
12. Borg, O. A.; Liu, Y. J.; Persson, P.; Lunell, S.; Karlsson, D.; Kadi, M.; Davidsson, J. *J. Phys. Chem. A* **2006**, *110*, 7045.
13. Murdock, D.; Crow, M. B.; Ritchie, G. A. D.; Ashfold, M. N. R. *J. Chem. Phys.* **2012**, *136*, 124313.
14. Paul, D.; Kim, H. K.; Hong, K.; Kim, T. K. *Bull. Korean Chem. Soc.* **2011**, *32*, 659.
15. Ichimura, T.; Mori, Y.; Shinohara, H.; Nishi, N. *Chem. Phys.* **1994**, *189*, 117.
16. Hwang, H. J.; El-sayed, M. A. *J. Chem. Phys.* **1992**, *96*, 856.
17. Park, M. S.; Jung, Y. J.; Lee, S. H.; Kim, D. C.; Jung, K. H. *Chem. Phys. Lett.* **2000**, *322*, 429.
18. Eppink, A. T. J. B.; Parker, D. H. *Rev. Sci. Instrum.* **1997**, *68*, 3477.
19. Zare, R. N.; Herschbach, D. R. *Proc. IEEE* **1963**, *51*, 173.
20. Ichimura, T.; Mori, Y.; Shinohara, H.; Nishi, N. *J. Chem. Phys.* **1997**, *107*, 835.
21. Han, K. L.; He, G. Z. *J. Photoch. Photobio. C* **2008**, *8*, 55.
22. Kim, T. K.; Park, M. S.; Lee, K. W.; Jung, K. H. *J. Chem. Phys.* **2001**, *115*, 10745.